Published in final edited form as:
J Electron Spectros Relat Phenomena. 2009 March 1; 170(1-3): 4–12. doi:10.1016/j.elspec.2008.10.008.

An assessment of the resolution limitation due to radiation-damage in x-ray diffraction microscopy

M. R. Howells[1,6], **T. Beetz**[2,*], **H. N. Chapman**[3,%], **C. Cui**[1,$], **J. M. Holton**[1,4], **C. J. Jacobsen**[1,2], **J. Kirz**[1,2], **E. Lima**[2,#], **S. Marchesini**[1], **H. Miao**[2], **D. Sayre**[2], **D. A. Shapiro**[1], **J. C. H. Spence**[1,5], and **D. Starodub**[5]

[1] Advanced Light Source, Lawrence Berkeley National Laboratory, 1 Cyclotron Rd., Berkeley, CA 94720 USA

[2]Department of Physics, State University of New York, Stony Brook, NY 11794, USA

[3]Lawrence Livermore National Laboratory, 7000 East Ave., Livermore, CA 94550, USA

[4]Department of Biochemistry and Biophysics, University of California, San Francisco, CA 94158-2330, USA

[5]Department of Physics and Astronomy, Arizona State University, Tempe, AZ 85287-1504, USA

Abstract

X-ray diffraction microscopy (XDM) is a new form of x-ray imaging that is being practiced at several third-generation synchrotron-radiation x-ray facilities. Nine years have elapsed since the technique was first introduced and it has made rapid progress in demonstrating high-resolution three-dimensional imaging and promises few-nm resolution with much larger samples than can be imaged in the transmission electron microscope. Both life- and materials-science applications of XDM are intended, and it is expected that the principal limitation to resolution will be radiation damage for life science and the coherent power of available x-ray sources for material science. In this paper we address the question of the role of radiation damage. We use a statistical analysis based on the so-called “dose fractionation theorem” of Hegerl and Hoppe to calculate the dose needed to make an image of a single life-science sample by XDM with a given resolution. We find that for simply-shaped objects the needed dose scales with the inverse fourth power of the resolution and present experimental evidence to support this finding. To determine the maximum tolerable dose we have assembled a number of data taken from the literature plus some measurements of our own which cover ranges of resolution that are not well covered otherwise. The conclusion of this study is that, based on the natural contrast between protein and water and “Rose-criterion” image quality, one should be able to image a frozen-hydrated biological sample using XDM at a resolution of about 10 nm.

6Corresponding author: mrhowells@lbl.gov, phone 510 486 4949, fax 510 486 7696.
*Now at Xradia, Inc., 4075 Sprig Dr., Concord, CA 94520 USA
%Now at Centre for Free-Electron Laser Science, U. Hamburg/DESY, Notkestrasse 85, 22607 Hamburg, Germany
$Now at Department of Physiology and Biomedical Engineering, Mayo Clinic College of Medicine, Rochester MN 55905, USA
#Now at Brookhaven National Laboratory, Upton NY 11973, USA

Keywords

Coherent x-rays; diffraction imaging; radiation damage; dose fractionation; frozen-hydrated samples

Introduction

X-ray diffraction microscopy (XDM) is a new form of x-ray imaging that is now being practiced by the authors at the Advanced Light Source x-ray facility at Berkeley [29,30]. Similar work has been going on at the synchrotron-light sources at Brookhaven [35,3], Argonne [45,61], Villigen [46], Grenoble [2], Berlin [52] and the SPring 8 facility in Japan [34,37] [36]. A short account of the early development work with many references is given by Spence and Howells [59]. The method works in both 2D and 3D and can be adapted for both life [3] and materials sciences. The images are generated in three steps; (1) diffraction patterns are recorded using coherent x-rays (just one for 2D or a tilt series for 3D) which provides the amplitudes of the diffracted wave field, (2) the phases of the wave field are obtained using variants of phase-retrieval algorithms developed outside of x-ray optics [8,9,13] and the image is recovered by means of a Fourier transform.

This form of x-ray imaging was first suggested by Sayre [49] and first demonstrated at Brookhaven in 1999 by Miao, Charalambous, Kirz and Sayre [35]. The latter experiment achieved a resolution of 75 nm using 0.73 keV x-rays and subsequent 2D experiments have pushed that value down to 7 nm measured in the image [37]. Our own XDM experiments have been done in the energy region 0.5–0.8 keV while other workers have used energies up to 8 keV. Some of the above-mentioned groups have achieved 3D imaging and the 3D resolution is now beginning to approach the 2D. In our experiments using radiation-hard samples we have reconstructed 3D images at 10 nm resolution of both test objects [29,30] [7] and a tantalum-oxide aerogel particle [1], both about 2 μm in size. We have also recorded diffraction patterns at 750 eV of freeze dried yeast and have reconstructed XDM images in 2D and stereo pair [54] but not 3D from them. The expansion of interest in the technique and the progress in developing its performance has been rapid and we are lead to investigate the fundamental limits to the resolution of this form of microscopy. It appears that the limit for life-science samples will be set by radiation damage, while for more-radiation-hard materials-science samples it will be set by the coherent power of available x-ray sources.

In this paper we address the question of the role of radiation damage in setting a resolution limit to life-science imaging by XDM. This is important because XDM is expensive (it needs at least an undulator on a third-generation synchrotron source) and if it is to have a niche in which it delivers unique and useful results, then it must produce performance beyond the limits of other microscopes. In this work, we are mainly interested in frozen-hydrated samples and we will refer to the practice of fast freezing the sample and holding it at low temperature for imaging, as “cryo-protection”. Such protection is used, for example, by the Munich group in their “electron-cryotomography” system [33] which has demonstrated a 3D resolution of 5-6 nm for biological samples of thickness 0.3-0.6 μm. Further analysis by the same group [42] has indicated that, although the resolution may eventually be improved by a factor of 2-3, the thickness has reached a fundamental limit caused by multiple electron scattering. For XDM such a thickness limit would not apply and we would expect to be able to make 3D images of whole cells in the size range from 0.5 μm to say 10-20 μm. Thus the main question we are addressing is: at what resolution can such images be made? A more fundamental reason why the issue of resolution is important in these investigations is that the resolution achieved by the Munich group is beginning to enable protein molecules of known structure in the sample to be recognized. The potential for determining the way in which these proteins “dock” together and

thus for throwing light on their function in molecular machines is an exciting general goal of these types of ultramicroscopy.

The question of calculating how much dose is *required* for imaging in a given microscope at a given resolution and statistical accuracy is essentially a statistical calculation. Such calculations have been presented before for x-ray microscopy in general [25,48,51] and also for XDM [29,50,56]. On the other hand the question of how much dose can the sample *tolerate* before unacceptable degradation occurs to images at a given resolution is not a matter of statistics but rather of radiation chemistry and biology. We thus arrive at two important quantities that we need to know about in order to estimate the dose-limited resolution, the *required dose for imaging* and the *maximum tolerable dose*. Obviously experiments can only be successful if the dose employed is greater than the required dose for imaging and less than the maximum tolerable dose.

In what follows we will use various techniques to estimate the required dose for imaging and the maximum tolerable dose. For the required dose we will use an estimation method based on the so-called dose fractionation theorem [20,32] which we explain below. To use the theorem for a 3D diffraction experiment one needs to know the scattering strength of a single voxel. This cannot normally be measured but we will describe simple methods by which it can be calculated and will compare the dose-resolution scaling law that results with our own XDM measurements. The maximum tolerable dose cannot be estimated by a simple calculation so it needs to be inferred from experimental results. We discuss below various experiments by ourselves and others that may be able to provide information. Since no 3D images of biological samples have yet been made by XDM, we try to make the best use of results from other types of experiment, 2D XDM, x-ray and electron crystallography and conventional electron and x-ray microscopy. Using these methods we will make estimates of the future capability of XDM based on the presently-available evidence.

The dose fractionation theorem

The theorem that we will use to simplify our calculation of the required dose for imaging was first proved by Hegerl and Hoppe [20]. According to these authors “A three-dimensional reconstruction requires the same integral dose as a conventional two-dimensional micrograph provided that the level of (statistical) significance and the resolution are identical”. The discussion provided by the originators of the theorem was largely in terms of a single voxel but, as pointed out by McEwan, Downing and Glaeser [32], the conclusion can be immediately generalized to a full 3D object by recognizing that conventional tomographic reconstructions are *linear* superpositions of the contributions of the individual voxels. A similar argument can be used to show that the theorem is applicable to XDM. McEwan et al also showed by computer simulations that the validity of the theorem could be extended to include experimentally realistic conditions of high absorption, signal-dependent noise, varying contrast and missing angular range. The practical meaning of the theorem is that the minimum dose that it specifies for a particular 3D imaging task can be shared (fractionated) among the views. This means that individual views will have very poor statistics, but still, according to McEwan et al, sufficient for alignment of the views by correlation methods.

We consider a single voxel of size $d \times d \times d$ and of the type that we would reconstruct in a fully 3D experiment, which means one with the same width in all three dimensions. In order to apply the theorem to predict the “required dose for imaging”, we need to know the dose required in an XDM experiment on the *single voxel alone* for an interesting range of values of d. It would be extremely hard to do such a series of experiments in practice. However, since the one-voxel experiments are simple in principle, it is easy to obtain their results by theoretical analysis which is what we do below. We will study a voxel which corresponds to correct sampling for

resolving a smallest spatial period of $2d$ in each coordinate direction (roughly similar to a Rayleigh resolution of d in standard microscopy). If the diffraction data are phased perfectly, this dose will also give the x-ray count in the corresponding voxel in the real-space computer reconstruction of the sample density.

To obtain the dose required for the one-voxel experiment we begin by calculating the x-ray coherent scattering cross section (σ_s) of the voxel for scattering into a detector with the right solid-angle collection to get the resolution d. This gives the dose required to get a given number of x-rays scattered by the voxel into the detector. The optical properties of the feature including the real and imaginary parts of its refractive index $\tilde{n} = 1-\delta-i\beta$, the intensity absorption coefficient μ, and the complex electron density ρ (given by $2\pi r_e\tilde{\rho} = (2\pi/\lambda)^2\,(\delta + i\beta)$ where r_e is the classical electron radius), that we will need, can be obtained from the tabulated optical constants. This is described, for example, in the review article by Kirz et al [26] equations 17, 18, 23 and 19 respectively. Furthermore, since we are particularly interested in the "excess" electron density of protein relative to a background of water, we define a relative density $\tilde{\rho}_r$ given by $2\pi r_e\tilde{\rho}_r = (2\pi/\lambda)^2\,\{(\delta-\delta_0) + i(\beta-\beta_0)\}$ where subscript zero refers to the background material. By this means we effectively encode the contrast between a feature and the background into the quantity $\tilde{\rho}_r$.

Calculation of the coherent scattering cross section of the voxel

Suppose the voxel is of amplitude transparency T surrounded by empty space of transparency unity. The Babinet inverse of this scattering object is an aperture of transparency $1-T$ in an opaque screen. Babinet's Principle asserts that, outside the (small) area of the incident beam, the diffraction pattern of these two objects is the same. The diffracted intensity at distance z is most easily calculated for the second object [18] as follows.

$$I(x,y)\frac{I_{\text{in}}|1T|^2d^4}{\lambda^2z^2}\text{sinc}^2\left(\frac{xd}{\lambda z}\right)\text{sinc}^2\left(\frac{yd}{\lambda z}\right)$$

The numerical aperture required to resolve a spatial period $2d$ is $\lambda/(2d)$ so the full width of the detector in both x and y should be $w = \lambda z/d$. Thus

$$\frac{\sigma_s}{d^2}\frac{\text{scattered energy}}{\text{incident energy}} \cong \frac{I(0,0)w^2}{I_{\text{in}}d^2}\frac{I_{\text{in}}|1-T|^2d^4}{\lambda^2z^2}\left(\frac{\lambda z}{d}\right)^2\frac{1}{I_{\text{in}}d^2}=|1-T|^2$$

showing that $\sigma_s = |1 - T|^2\,d^2$ which is in agreement with equation 23 of [38] for example, as well as being intuitively reasonable. To get the complex absorbency, $1 - T$ in terms of the material properties of the voxel we use Kirz 1995 [26] equation (20) for the wave amplitude ψ

$$\psi=\psi_0e^{-2\pi i\tilde{n}d/\lambda}=\psi_0e^{-2\pi i(1-\beta-i\delta)d/\lambda}=\psi_0e^{-2\pi id/\lambda}e^{-2\pi\beta d/\lambda}e^{2\pi i\delta d/\lambda}\text{whence}$$
$$T=e^{-2\pi\beta d/\lambda}e^{2\pi i\delta d/\lambda}\cong 1-2\pi d(\beta+i\delta)/\lambda$$

where we have introduced the weak-phase-weak-amplitude approximation (which will usually be valid for a resolution element which is intrinsically small). Recasting this in terms of the complex electron density $\tilde{\rho}$, (Kirz 1995 [26] equation 19), we have

$$|1-T|^2=(2\pi d)^2|\beta+i\delta|^2/\lambda^2=d^2r_e^2\lambda^2\left|\tilde{\rho}_r\right|^2$$

and finally

$$\sigma_s=|1-T|^2d^2=r_e^2\lambda^2\left|\tilde{\rho}_r\right|^2d^4 \quad (1)$$

Thus σ_s scales as the voxel size to the fourth power. As we will see this leads to an inverse fourth-power scaling of the dose with d. The scaling with wavelength is dominated by the lamda-squared term, especially at wavelengths $\ll$ 2 nm where the atomic scattering factors of the light elements approach a constant value.

Equation (1) is important to our argument and we have checked it in various ways. Firstly, we took the differential scattering cross section of a single electron, integrated it over the detector solid angle required to get resolution d and summed it coherently over the effective number of electrons in our voxel. Secondly we used literature calculations of the cross section of spherical particles of the same size as our voxel [23, 28]. The three expressions so obtained agreed with equation (1) up to a constant factor of order one. We may also argue that the contrast (C) between the voxel and vacuum scales as the thickness, i. e. as d. The Rose criterion (see later) says that the number of incident x-rays per unit area, N_0, which is proportional to the dose, must satisfy $N_0d^2 > 25/C^2$. Therefore, since C scales as d, N_0 scales as $1/d^4$.

Relation between flux density and dose

Before proceeding to calculate the dose for our case we first make some definitions and show how the dose is related to the number of incident particles per unit area. This relationship will be needed in order to compare published data with different incident particles. For x-rays of energy $h\nu$, we know that for any object (with density ε), the number of transmitted x-rays per unit area N at depth t due to an incident number per unit area N_0 is given by $N = N_0 \exp(-\mu t)$ whence the *energy* deposition per unit volume at the surface, $[\partial(Nh\nu)/\partial t]_{t=0}$, is $\mu N_0 h\nu$. Therefore the surface dose D (energy deposited per unit mass) is

$$D=\mu N_0 h\nu/\varepsilon. \quad (2)$$

D will be in Gray (J/kg) if the other quantities are in MKS units. The last equation relates the incident particle flux density to the dose for given material parameters irrespective of d. It is based on the conservative assumption that 100% of the energy deposited contributes to the dose, i. e. no photoelectrons escape. Some numerical values for protein are given in Fig. 1.

In the case of illumination by an electron beam, the energy deposited per unit length of trajectory (and thence per unit volume) is given by the Bethe formula, (see for example equation 10.2 of [44]). We have used this to convert the dose given in electrons per unit area in some literature reports to the corresponding dose in Gray.

Estimation of the dose and calculation of the required imaging dose

We want to estimate the dose D (Gy) and the number of incident x-rays per unit area N_0 required to get a given number P of x-rays scattered into the detector from the given voxel. (The choice

of P will be determined by the statistical accuracy required from the measurement.) The total number of photons incident on the voxel (the fluence) is $N_0 d^2$ of which a fraction σ_s/d^2 will be scattered into the detector. Therefore the requirement is for $N_0 = P/\sigma_s$ which, from equations (1) and (2), leads to

$$D=\frac{\mu Ph\nu}{\varepsilon\sigma_s}=\frac{\mu Ph\nu}{\varepsilon}\frac{1}{r_e^2\lambda^2\left|\tilde{\rho}_r\right|^2 d^4}. \tag{3}$$

and

$$N_0=\frac{P}{r_e^2\lambda^2\left|\tilde{\rho}_r\right|^2 d^4} \tag{4}$$

As examples we show the fluence and dose curves (Fig. 2 (a) and (b)) for a protein sample of empirical formula $H_{50}C_{30}N_9O_{10}S_1$ and density 1.35 gm/cm^3 as a function of x-ray energy. The curves are for a voxel size (resolution) of 10 nm and statistical accuracy based on the Rose criterion [47]. The latter is an experimentally-based criterion for reliable detectability of a feature against background noise. The requirement is generally that the feature signal should be five times greater than the rms noise of the background. When the noise is the shot noise of the feature signal itself then it is conventional to set the particle count equal to 25. The curve for the required fluence (Fig. 2(a)) is dominated by the λ^{-2} scaling of the cross section. This argues for using the longest possible wavelength for these experiments. On the other hand the wavelength should be shorter than, say, a quarter to a half of the resolution so that the diffraction angle is not too large, and short enough that the sample is a weak absorber (< 20%, say), so that data analysis can proceed on the basis of the Born approximation. Unlike the required fluence, the required dose does not show strong energy dependence above about 1 keV. This is because the roughly $\lambda^{5/2}$ scaling of the absorption coefficient tends to cancel the wavelength dependence of $h\nu/\sigma_s$ in equation (3). Equation (3) also allows the calculation of the "required dose for imaging" as a function of resolution d. We have evaluated that for protein against a background of water for 1 keV and 10 keV as shown by the continuous straight lines in Fig. 3. One can see that the change in dose from 1 keV to 10 keV is not very significant.

Also from (3) the resolution scaling of the dose is seen to be $1/d^4$ and is determined entirely by the cross section. Now applying the dose fractionation theorem we may say that the *same dose* will be required to measure the same $d\times d\times d$ voxel to the same statistical accuracy in a 3D tomography experiment. Hence, the inverse-fourth-power scaling with d, will also apply to a 3D sample.

These calculations have been revisited recently by some of the present authors [60] in the context of serial crystallography. Essentially the same calculation was presented but without use of the dose fractionation theorem. The functional dependence of all of the above results, including the $1/d^4$ scaling, were confirmed although with different numerical prefactors. It is important to note that both of these calculations have used similar idealized forms of the sample: in our case that the chosen voxel is *typical* and in Starodub's that the sample density is *constant* within a given boundary. In neither case were the detailed structures that one would find in a real sample taken into account. Thus we can only expect that the measured values of the dose-resolution scaling, that we will report in the next section, will follow an approximate $1/d^4$ scaling. Starodub et al also point out that the number of x-rays needed for 3D phase

retrieval may be considerably more than that needed for the standard geometrical-optical tomography.

We note that the inverse fourth-power scaling described above, which is based on coherent diffraction, appears to be in disagreement with the third-power scaling derived by Shen and coworkers [56] on the basis of incoherent diffraction. However, in our view, the disagreement is only apparent and both calculations can be shown to be correct but belonging to different regimes. It is fairly well-known that all hard x-ray scattering becomes effectively incoherent at angles (θ) that are sufficiently wide that the scattering features are at an atomic length scale: $\theta \sim \lambda/a$ where a is the size of an atom. The recorded intensity is then the result of a "random-walk" type of phasor summation in which the phase differences are large and the coherent cross terms tend to average to zero. On the other hand where the scattering features are larger and the angles smaller ($\theta \sim \lambda/d$), where d is a few nm or more, then we can use a macroscopic treatment based on refractive index, the phase differences will be smaller and a coherent phasor superposition will be appropriate. Figure 3 in the review by Bergh et al [4] shows a helpful example in which feature sizes above 10 nm are shown to be in the coherent regime, those below 1 nm in the incoherent regime and those between 1 and 10 nm in a transition regime. We justify our use of the coherent treatment in this work on the basis that it corresponds more closely with the feature size that we think is likely to be resolved in XDM experiments, especially those on life-science samples.

Another important consideration is that the fluence, predicted by Fig. 2(a) to be required for a 10 nm XDM experiment on protein against a background of water, needs to be delivered to the sample as a coherent x-ray beam. Part of the attraction of XDM is that such coherent x-ray beams are already available from undulators on present-generation synchrotron-radiation sources such as the Advanced Light Source at Berkeley USA. For example our present tomographic experiments are done with exposure times of several tens of seconds per view using a general-purpose beam line. The use of a purpose-designed beam line plus the soon-to-be-completed ALS upgrade would improve that by a factor of about a thousand.

Measurements of the required imaging dose

In order to test the calculations of the required imaging dose we have carried out the following series of measurements on freeze-dried yeast cells. The cells are about 2 μm in size and, as always in XDM, only a single sample surrounded by blank space is exposed. Standard XDM diffraction patterns were recorded using a series of exposure times that increased on a logarithmic grid. The general technique for doing this is described for example by Beetz et al and Shapiro et al [3], [54] and a typical pattern is shown in Fig 4(a). The patterns were analyzed by first taking an azimuthal average so as to produce a relation between diffracted signal and spatial frequency (Fig. 4(b)). A cut-off frequency was then determined from where the diffracted signal reached the noise floor of the detection process, allowing a relationship between normalized exposure time (representing dose) and normalized cut-off frequency (representing resolution) to be obtained. We show two examples of this type of relationship in Fig. 4(c). The straight part of the lower curve has a slope of −3.9, close to the value of −4 derived for the idealized samples. The straight-line behavior means that the resolution is improving systematically, commensurate with the increasing number of incident x-rays. Obviously this cannot go on forever and eventually damage must begin to occur and the gains in resolution must slow down and stop. This would be represented by an upturn at the high-dose end of the straight line graph (whether or not the slope is exactly −4). We see that in the lower curve of Fig. 4(c) there is such an upturn, so we conclude that damage-induced degradation of the resolution has indeed begun to occur. The upper curve shows slightly different behavior. Its straight portion has a slope of −4.7 which is somewhat different from the idealized samples but this is to be expected for reasons explained in the previous section.

The general pattern has been that most of the slope measurements were fairly close to −4 but with some departures within the range (−4 ± 1) However, it also shows the beginning of an upturn at the maximum dose which we again ascribe to the onset of damage. Indeed, we believe that the departure from the straight lines in plots like Fig. 4(c) could be used as a quantitative means of monitoring the onset of damage.

To put this type of measurement in context we can convert the exposure times to dose units and the cutoff frequencies to spatial half-periods giving a relation between dose in Gy and resolution in nm. Two such curves, representing measurements made on freeze-dried yeast, are plotted in Fig. 3 (crosses). This shows good agreement with the predicted magnitude. Remember however that the predicted magnitude is for frozen-hydrated material so the precise agreement shown should not be taken too seriously.

Measurement of the maximum tolerable dose

Since the nineteen seventies [15], there has been strong interest in understanding the role of radiation damage in various forms of imaging of life-science samples. This has been important in direct imaging by electron and x-ray microscopes and in reconstructive imaging by methods such as the single-particle technique [10] and by x-ray and electron crystallography. During this time there has been a continual growth in the power of electron and x-ray sources and an interest in using smaller crystals in crystallography and larger numbers of images in single-particle work, all of which has generated a motivation to push data collection to the limits allowed by damage. Thus radiation damage studies are still very much on the current agenda (see for example, the comments of Henderson [22] and reviews of a series of international workshops on the subject [11,12,39,43]. Our task is to judiciously apply the latest information from these studies to the issue of determining the maximum tolerable dose for XDM.

The resolution in life-science XDM is desired to be 3-10 nm although currently expected to be greater than 10 nm (see later). This does not correspond to the resolution goals in x-ray or electron crystallography where much higher resolution levels that may lead to atomic-resolution structure determinations, are usually desired. In fact a significant part of the x-ray damage literature refers to *primary* damage; that is damage to the highest resolution structures and not to structures in the three-to-ten-plus nm range of interest to us. Nevertheless we have found reports in the crystallography literature that have at least some reference to damage at resolution values in our range of interest and also give quantitative spot-fading data. We have also added information from other imaging methods; electron tomography and single-particle measurements as well as a few results from XDM and x-ray microscope experiments to the compilation in Table 1 and Fig. 3.

Although the data from the literature noted above give quite a consistent picture as between electron and x-ray measurements (as noted by Henderson [21]), the x-ray measurements have a large gap in the resolution region of principal interest to us. This led us to carry out spot-fading measurements ourselves using beam line 8.3.1 at the Advanced Light Source at Berkeley. The experiments were done by J. M. Holton using the established crystallography facilities of the beam line with a ribosome crystal grown by Dr A. Vila-Sanjurjo in the laboratory of Prof. J. Cate of University of California Berkeley. The total exposure at 10 keV x-ray energy was about 24 hours with high-dose-rate (wide-slit) exposures to do damage alternated with low-dose (narrow-slit) exposures to measure the spots. The spot patterns at the beginning, middle and end of this sequence are shown in Fig. 5 and the whole process can be seen as a movie at http://bl831.als.lbl.gov/~jamesh/ribo_blast/diffraction.gif. The following points can be noted.

- The crystal has a unit cell size a=b=685 Å, c=2690 Å with space group probably I4122. It diffracted out to about 10Å when it was undamaged.

- As the dose increased, the intensity of the Bragg spots faded, without increase of the spot size (signifying preservation of the long-range order), starting from the highest-resolution spots.
- As the intensity in the (high-angle) Bragg spots diminished, that in the central (small-angle) pattern increased, eventually very strongly.
- The number and resolution of the spots which faded for each increment of the dose was quantified by the DISTYL software [62] as listed in Table 1 and Fig. 3.
- As shown in Fig. 3 the new results are consistent with the earlier ones from crystallography and imaging by both electrons and x-rays. Taken together, the data in the resolution range 0.1–10 nm suggest an approximate straight line on the log-log plot with slope corresponding roughly to the following linear relationship:

$$\text{Dose(Gy)} = 1.0 \times 10^8 \times \text{Resolution(nm)} \quad (5)$$

Finally we turn to the remaining data above resolution 10 nm. There are only three data points, one from soft x-ray CXDI and the others from soft x-ray zone-plate microscopy.

There have recently been two more studies published [27,41] (since the original submission of this manuscript) that report data that can be compared to our Fig. 3 and equation (5) as reviewed by Holton [24]. Applying an exponential decay of Bragg intensity, with the dose at half-maximum intensity being given by equation (5), to the squared structure factors of apoferritin (Protein Data Bank ID: 2clu) results in a remarkably linear falloff of total intensity with dose that reaches half at 42 MGy. This is consistent with the 43 ± 3 MGy observed at half total intensity by Owen and Garman [41]. Moreover, scaling these same exponentially modified data to unmodified intensities as described by Kmetko et al. [27] yields a “sensitivity factor” that is identical to the one they reported for their apoferritin observations. Our proposed estimate of the maximum tolerable dose: 1.0×10^8 Gy per nm of resolution therefore appears remarkably consistent with more recent damage studies, and can be used as a rule of thumb for predicting how long spots of a given d-spacing will last.

The meaning of data summarized in Fig. 3

The data summarized in Fig. 3 refer to two different dose levels; the *required dose for imaging* (the two continuous black lines and associated dashed lines going downhill to the right), and the *maximum tolerable dose*, represented by various isolated points forming a rough straight line going uphill to the right, indicated by the wide gray line. On the left-hand side of the 10 nm crossover of the two lines it is obvious that the required dose for imaging by XDM becomes several orders of magnitude greater than the maximum tolerable dose. This reflects the fact that XDM experiments, which use *only one sample*, cannot be done at those resolution values. It is well known in the crystallography community that one can solve structures at resolutions much less than 10 nm by using a crystal or crystals containing enormous numbers of copies of the sample. The large dose involved can then be shared among the many copies and the experiment becomes feasible without exceeding the maximum allowed dose. Similarly single-particle cryo-electron microscopy synthesizes the image of one molecule by computationally forming a virtual “crystal” from many input images. Evidently both these schemes require that many copies of the sample can be made and perhaps crystallized. On the other hand when the interesting objects are either scarce or are not identical or cannot be crystallized, XDM can still be considered. In short XDM is a *microscope*.

Given that XDM experiments can only be successful if the dose employed is greater than the required dose for imaging and less than the maximum tolerable dose, we can see that the region of the graph in Fig. 3 where XDM experiments could be expected to be successful is the triangular region between the two lines to the right of the crossover. The best resolution in the "good" region is evidently at the crossover of the two "lines". Thus we see that the best resolution predicted for simple XDM based on the natural contrast between protein and water, is about 10 nm which is a principal result of our investigation. Given this result and our conviction that future XDM images of resolution less than 1 nm are unlikely (even with radiation-hard samples), we have truncated the required-dose-for-imaging graph in Fig. 3 at 1 nm.

Circumventing the 10-nm damage limit in XDM

The 10-nm resolution limit in XDM is based on the natural x-ray contrast between protein and vitreous ice. This suggests that the resolution limit can be improved by contrast enhancing strategies. For example if we introduce a contrast agent, which has higher electron density than protein, that will increase the value of $\tilde{\rho}_r$ by some factor f say, then equation (3) shows that the required dose will go down by a factor f^2. This approach must be used with caution because it may introduce artifacts but it provides an opportunity for specific labeling which may add important information.

Another approach is to use samples that are in forms where there is some prior knowledge about their structure. The "molecular replacement" method, which uses known proteins of similar sequence to assist phasing of new structures, might be applicable here. Other examples could be a sample with unknown components in a known spatial arrangement such as a periodicity (e. g. fibers or helical structures) or an object with known components such as macromolecules in an unknown spatial arrangement (a molecular machine say). Either way the prior knowledge reduces the amount of information to be provided by x-ray diffraction and hence also the needed number of x-rays.

Ways around the damage limit using multiple copies of the sample

If multiple copies, but not crystals, are available there still several pathways to higher resolution than the "single-sample" limit that applies to XDM. We mentioned image reconstructions by the single-particle method earlier. We can add to that small-angle solution scattering which also provides higher-resolution structural information (although not yet images). However, in addition to these established approaches, we mention two promising new ideas.

It has been demonstrated experimentally that bioparticles can be aligned by fluid flow and by electric and magnetic fields. Therefore, a continuous single-file stream of aligned particles running across a continuous X-ray beam can be created and can produce useful x-ray diffraction data [58]. Particle movement does not affect the diffraction pattern, and the constant refreshment of the particles avoids all damage. Preliminary results have been obtained recently from protein nanocrystals [55]. Finally, it has been suggested that a sufficiently brief X-ray pulse can terminate before damage occurs, yet, if provided by an X-ray laser, can also provide sufficient photons for a useful "elastic" diffraction pattern [40]. The duration of such a pulse would need to be comparable with the Auger recombination time of a few femtoseconds, much shorter than the Debye nuclear motion period. Experiments confirming this "diffract then destroy" principle have been published using soft X-rays at low resolution [6].

Conclusion

The principal conclusion of this paper is that for unique, frozen-hydrated biological objects with only natural x-ray contrast the resolution of XDM at Rose-criterion image quality will be

limited by radiation damage to be not better than 10 nm. We have also shown that the scaling law for the required dose for imaging as a function of resolution (*d*) is approximately $1/d^4$. Our measurements and compilation of results from the literature has revealed an interesting underlying approximately linear relationship between the maximum allowed dose (defined as 50% spot fading) and the resolution, with the allowed dose being equal to 1.0×10^8 Gy per nm of resolution. We have shown that this estimate is in good agreement with other recently published estimates. We have made a case that the 10-nm limit is not insurmountable and have gaven examples of strategies for circumventing it.

Acknowledgments

The authors are grateful to Dr A. Vila-Sanjurjo and Prof. J. Cate for permission to use the ribosome crystal, to Prof. R. M. Glaeser for extended and valuable discussions and comments and to Dr. H. A. Padmore for sustained encouragement of this work. The Lawrence Berkeley National Laboratory authors and the Advanced Light source facility at Lawrence Berkeley National Laboratory are supported by the Director, Office of Energy Research, Office of Basics Energy Sciences, Materials Sciences Division of the U. S. Department of Energy, under Contract No. DE-AC03-76SF00098. J. M. Holton is additionally supported by National Institutes of Health (NIH) grant numbers 5U54 GM074929-02 and 1P50 GM082250-02. The work of the LLNL authors was performed under the auspices of the U.S. Department of Energy by University of California, Lawrence Livermore National Laboratory under Contract W-740740 5-Eng-48. The Stony Brook group has been supported by NIH grant number 1R01 GM64846-01, and by U. S. Department of Energy grant number DEFG0204ER46128. ASU work supported by NSF award IDBR 0555845

References

1. Barty A, Marchesini S, Chapman HN, Cu C, Howells MR, Shapiro DA, Minor AM, Spence JCH, Weierstall U, Noy JI, Hau-Riege SP, Artyukhin AB, Baumann T, Willey T, Stolken J, vanBuuren T, Kinney JH. Three-Dimensional Coherent X-Ray Diffraction Imaging of a Ceramic Nanofoam: Determination of Structural Deformation Mechanisms. Phys Rev Lett 2008;101:055501. [PubMed: 18764404]
2. Baruchel J, Bleuet P, Bravin A, Coan P, Lima E, Madsen A, Ludwig W, Pernot P, Susini J. Advances in synchrotron hard X-ray based imaging. Comptes Rendus Physique 2008;9:624–641.
3. Beetz T, Howells MR, Jacobsen C, Kao CC, Kirz J, Lima E, Mentes TO, Miao H, Sanchez-Hanke C, Sayre D, Shapiro D. Apparatus for X-ray diffraction microscopy and tomography of cryo specimens. Nucl Instrum Meth A 2005;545:459–468.
4. Bergh M, Huldt G, Tîmneanu N, Maia F, Hajdu J. Feasibility of Imaging Living Cells at Sub-Nanometer Resolutions by Ultra-fast X-ray Diffraction. Quarterly Review of Biophysics. 2008 accepted.
5. Burmeister WP. Structural changes in a cryo-cooled protein crystal owing to radiation damage. Acta Cryst 2000;D56:328–341.
6. Chapman HN, Barty A, Bogan MJ, Boutet S, Frank M, Hau-Riege SP, Marchesini S, Woods BW, Bajt S, Benner WH, London RA, Plönjes E, Kuhlmann M, Treusch R, Düsterer S, Tschentscher T, Schneider JR, Spiller E, Möller T, Bostedt C, Hoener M, Shapiro DA, Hodgson KO, Spoel Dvd, Burmeister F, Bergh M, Caleman C, Huldt G, Seibert MM, Maia FRNC, Lee RW, Szöke A, Timneanu N, Hajdu J. Femtosecond diffractive imaging with a soft X-ray free-electron laser. Nature Physics 2006;2:839–843.
7. Chapman HN, Barty A, Marchesini S, Noy A, Riege SH, Cui C, Howells MR, Rosen R, He H, Spence JCH, Weierstall U, Beetz T, Jacobsen C, Shapiro D. High-resolution ab initio Three-dimensional X-ray Diffraction Microscopy. Journal of the Optical Society of America A 2005;23(5):1179–1200.
8. Elser V. Phase retrieval by iterative projections. J Opt Soc Am A 2003;20:40–55.
9. Fienup JR. Reconstruction of an object from the modulus of its Fourier transform. Opt Lett 1978;3(1): 27–29. [PubMed: 19684685]
10. Franck, J. Three-Dimensional Electron Microscopy of Macromolecular Assemblies. San Diego: Academic Press; 1996.
11. Garman E, Nave C. Radiation damage to crystaline biological molecules: current view. j Synchrotron Rad 2002;9:327–328.
12. Garman EF, McSweeney SM. Progress in research into radiation damage in cryo-cooled macromolecular crystals. J Synchrotron Rad 2007;14:1–3.

13. Gerchberg RW, Saxton WO. A practical algorithm for the determination of phases from image and diffraction plane pictures. Optik 1972;25:237–246.
14. Glaeser R, Faciotti M, Walian P, Rouhani S, Holton J, Macdowell A, Celestre R, Cambie D, Padmore H. Characterisation of conditions required for x-ray diffraction experiments with protein microcyrstals. Biophysical J 2000;78:3178–3185.
15. Glaeser RM. Limitations to significant information in biological electron microscopy as a result of radiation damage. Journal of Ultrastructure Research 1971;36:466–482. [PubMed: 5107051]
16. Glaeser RM. Private communication. 2004
17. Glaeser RM, Taylor KA. Radiation damage relative to transmission electron microscopy of biological specimens at low temperature: a review. Journal of Microscopy 1978;112:127–138. [PubMed: 347079]
18. Goodman, JW. An Introduction to Fourier Optics. McGraw-Hill; San Francisco: 1968.
19. Hayward SB, Glaeser RM. Radiation damage of purple membrane at low temperature. Ultramicroscopy 1979;4:201–210. [PubMed: 473421]
20. Hegerl R, Hoppe W. Influence of electron noise on three-dimensional image reconstruction. Zeitschrift für Naturforschung 1976;31a:1717–1721.
21. Henderson, R. Cryo-protection of protein crystals against radiation damage in electron and X-ray diffraction. Proceedings of the Royal Society of London; 1990. p. 6-8.
22. Henderson R. Realizing the potential of electron cryo-microscopy. Quarterly Reviews of Biophysics 2004;37:3–13. [PubMed: 17390603]
23. Henke BL, DuMond JWM. Submicroscopic structure determination by long wavelength x-ray diffraction. J Appl Phys 1955;26:903–917.
24. Holton J. A Beginner's Guide to Radiation Damage. Submitted to J Synchrotron Rad. 2008
25. Jacobsen, C.; Medenwaldt, R.; Williams, S. A perspective on biological x-ray and electron microscopy. In: Thieme, J.; Schmahl, G.; Umbach, E.; Rudolph, D., editors. X-ray Microscopy and Spectromicroscopy. Springer-Verlag; Berlin: 1998. p. II-93-102.
26. Kirz J, Jacobsen C, Howells M. Soft x-ray microscopes and their biological applications. Quarterly Reviews of Biophysics 1995;28(1):33–130. [PubMed: 7676009]
27. Kmetko J, Husseini NS, Naides M, Kalinin Y, Thorne RE. Quantifying X-ray radiation damage in protein crystals at cryogenic temperatures. Acta Cryst 2006;D62:1030–1038.
28. London RA, Rosen MD, Trebes. Wavelength Choice for Soft X-ray Laser Holography of Biological Samples. Appl Opt 1989;28:3397–3404.
29. Marchesini S, Chapman HN, Hau-Riege SP, London RA, Szoke A, He H, Howells MR, Padmore H, Rosen R, Spence JCH, Weierstall U. Coherent x-ray diffractive imaging: applications and limitations. Optics Express 2003;11(19):2344–2353. [PubMed: 19471343]
30. Marchesini S, He H, Chapman HN, Noy A, Hau-Riege SP, Howells MR, Weierstall U, Spence JCH. X-ray image reconstruction from a diffraction pattern alone. Phys Rev B 2003;68:140101(R).
31. Maser J, Osanna A, Wang Y, Jacobsen C, Kirz J, Spector S, Winn B, Tennant D. Soft x-ray microscopy with a cryo STXM: I. Instrumentation, imaging, and spectroscopy. Journal of Microscopy 2000;197:68–79. [PubMed: 10620150]
32. McEwen BF, Downing KH, Glaeser RM. The relevance of dose-fractionation in tomography of radiation-sensitive specimens. Ultramicroscopy 1995;60:357–373. [PubMed: 8525549]
33. Medalia O, Weber I, Frangakis A, Nicastro D, Gerisch G, Baumeister W. Macromolecular architecture in eukariotic cells visualized by cryoelectron tomography. Science 2002;298(8 Nov):1209–1213. [PubMed: 12424373]
34. Miao J, Chapman HN, Kirz J, Sayre D, Hodgson KO. Taking X-ray Diffraction to the Limit: Macromolecular Structures from Femtosecond X-Ray Pulses and Diffraction Microscopy of Cells with Synchrotron Radiation. Annu Rev Biophys Biomol Struct 2004;33:157–176. [PubMed: 15139809]
35. Miao J, Charalambous P, Kirz J, Sayre D. Extending the methodology of x-ray crystallography to allow imaging of micrometre-sized non-crystalline specimens. Nature 1999;400(22 July):342–344.

36. Miao J, Chen CC, Song C, Nishino Y, Kohmura Y, Ishikawa T, Ramunno-Johnson D, Lee TK, Risbud SH. Three-Dimensional GaN-Ga2O3 Core Shell Structure Revealed by X-Ray Diffraction Microscopy. Phys Rev Lett 2006;97:215503. [PubMed: 17155748]
37. Miao J, Ishikawa T, Johnson B, Anderson EH, Lai B, Hodgson KO. High resolution 3D x-ray diffraction microscopy. Phys Rev Lett 2002;89(8):088303, 1–4. [PubMed: 12190506]
38. Mueller, R. Holography. In: Jorna, S., editor. X-ray Laser Applications Study. Physical Dynamics Inc; La Jolla: 1976.
39. Nave C, Garman EF. Towards an understanding of radiation damage in cryocooled macromolecular crystals. J Synchrotron Radiation 2005;12:257–260.
40. Neutze R, Wouts R, vander-Spoel D, Weckert E, Hadju J. Potential for biomolecular imaging with femtosecond X-ray pulses. Nature Photonics 2000;406:752–757.
41. Owen RL, Rudino-Pinera E, Garman EF. Experimental determination of the radiation dose limit for cryocooled protein crystals. Proc Natl Acad Sci USA 2006;103:4912–4917. [PubMed: 16549763]
42. Plitzko J, Frangakis A, Nickell S, Forster F, Gross A, Baumeister W. In vivo veritas: electron cryotomography of cells. Trends in Biotechnology 2002;20(suppl 8):S40–S44.
43. Ravelli R, Garman EF. Radiation damage in macromolecular cryocrystallography. Current Opinion in Structural Biology 2006;16:624–629. [PubMed: 16938450]
44. Reimer, L. Transmission electron microscopy: physics of image formation and microanalysis. Berlin: Springer-Verlag; 1984.
45. Robinson IK, Vartanyants IA, Williams GJ, Pfeifer MA, Pitney JA. Reconstruction of the shapes of gold nanocrystals using coherent x-ray diffraction. Phys Rev Lett 2001;87(19):195505, 1–4. [PubMed: 11690423]
46. Rodenburg JM, Hurst AC, Cullis AG, Dobson BR, Pfeiffer F, Bunk O, David C, Jefimovs K, Johnson I. Hard-X-Ray Lensless Imaging of Extended Objects. Phys Rev Lett 2007;98:034801. [PubMed: 17358687]
47. Rose, A. Television pickup tubes and the problem of vision. In: Marton, L., editor. Advances in Electronics. New York: 1984. p. 131-166.
48. Rudolph, D.; Schmahl, G.; Niemann, B. Amplitude and Phase Contrast in X-ray Microscopy. In: Duke, PJ.; Michette, AG., editors. Modern Microscopies. Pergamon; Oxford: 1990. p. 59-67.
49. Sayre, D. Prospects for long-wavelength x-ray microscopy and diffraction. In: Schlenker, M.; Fink, M.; Goedgebuer, JP.; Malgrange, C.; Viénot, JC.; Wade, RH., editors. Imaging Processes and Coherence in Physics. Springer-Verlag; Berlin: 1980. p. 229-235.
50. Sayre D, Chapman HN. X-ray microscopy. Acta Cryst 1995;A51:237–252.
51. Sayre D, Kirz J, Feder R, Kim DM, Spiller E. Transmission microscopy of unmodified biological materials: comparative radiation dosages with electrons and ultrasoft x-ray photons. Ultramicroscopy 1977;2:337–341. [PubMed: 919076]
52. Schlotter WF, Rick R, Chen K, Schertz A, Stöhr J, Lüning J, Eisebitt S, Günter C, Eberhardt W, Hellwig O, McNulty I. Multiple reference Fourier Transform holography with soft x-rays. Appl Phys Lett 2006;89(16):163112.
53. Schneider G. Cryo x-ray microscopy with high spatial resolution in amplitude and phase contrast. Ultramicroscopy 1998;75:85–104. [PubMed: 9836467]
54. Shapiro D, Thibault P, Beetz T, Elser V, Howells M, Jacobsen C, Kirz J, Lima E, Miao H, Neiman A, Sayre D. Biological Imaging by Soft X-ray Diffraction Microscopy. Proc Natl Acad Sci USA 2005;102:15343–15346. [PubMed: 16219701]
55. Shapiro, DA.; Ponte, DD.; Doak, RB.; Fromme, P.; Hembree, G.; Hunter, M.; Marchesini, S.; Schmidt, K.; Weierstall, U.; Spence, JCH. Powder diffraction from a continuous microjet of nanoscale protein crystals. J Synch Rad. 2008. in pressp. Preprint - http://arxiv.org/abs/0803.4027
56. Shen Q, Bazarov I, Thibault P. Diffractive imaging of nonperiodic materials with future coherent X-ray sources. J Synchrotron Rad 2004;11:432–438.
57. Sliz P, Harrison SC, Rosenbaum G. How does radiation damage in protein crystals depend on x-ray dose. Structure 2003;11:13–19. [PubMed: 12517336]
58. Spence JCH, Doak RB. Single Molecule Diffraction. Phys Rev Lett 2004;92(19):198102. [PubMed: 15169448]

59. Spence, JCH.; Howells, MR. Coherent diffraction imaging with x-rays and electrons. Synchrotron Radiation Instrumentation: Eighth International Conference; San Francisco: American Institute of Physics Conference Proceedings; 2004.

60. Starodub D, Rez P, Hembree G, Howells M, Shapiro D, Chapman HN, Fromme P, Schmidt K, Weierstall U, Doak RB, Spence JCH. Dose, exposure time and resolution in serial X-ray crystallography. J Synchrotron Rad 2008;15:62–73.

61. Williams GJ, Pfeifer MA, Vartanyants IA, Robinson IK. Three-Dimensional Imaging of Microstructure in Au Nanocrystals. Phys Rev Lett 2003;90:175501, 1–4. [PubMed: 12786079]

62. Zhang Z, Sauter NK, vandenBedem H, Snell G, Deacon AM. Automated diffraction image analysis and spot searching for high-throughput crystal screening. J Appl Cryst 2005;39:112–119.

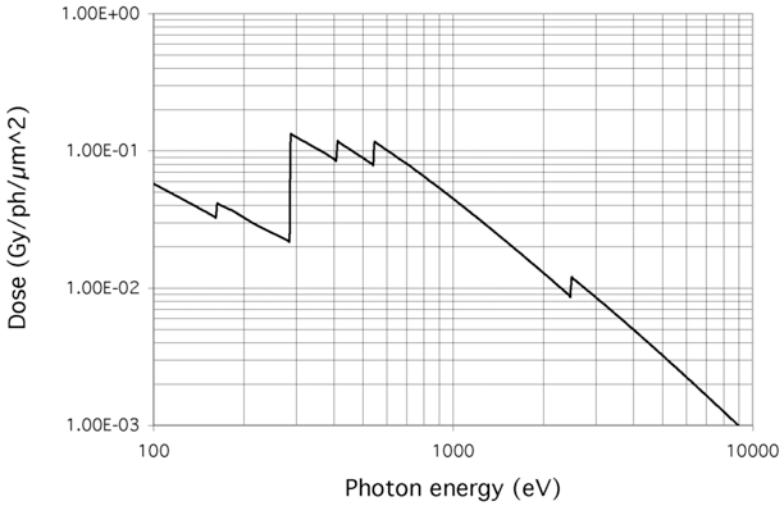

Fig. 1.

The surface dose in Gray for an incident x-ray fluence of 1 photon/μm^2 for a range of x-ray energies. The material is taken to be protein of empirical formula $H_{50}C_{30}N_9O_{10}S_1$ and density 1.35 gm/cm^3.

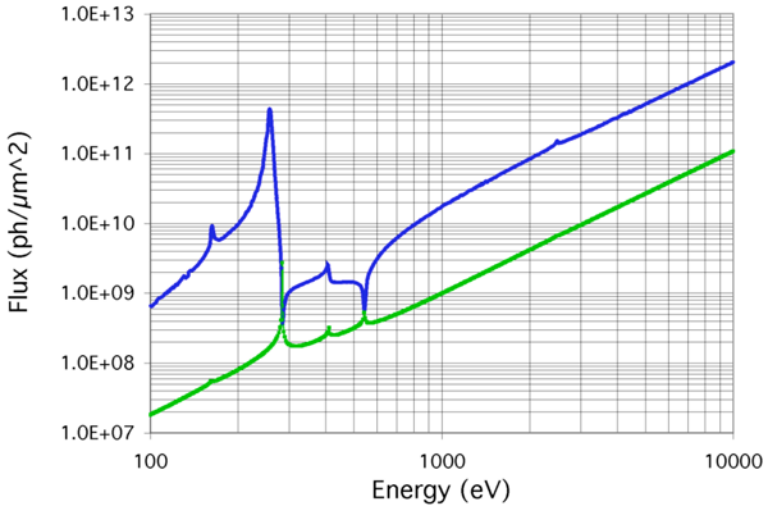

Fig. 2(a)

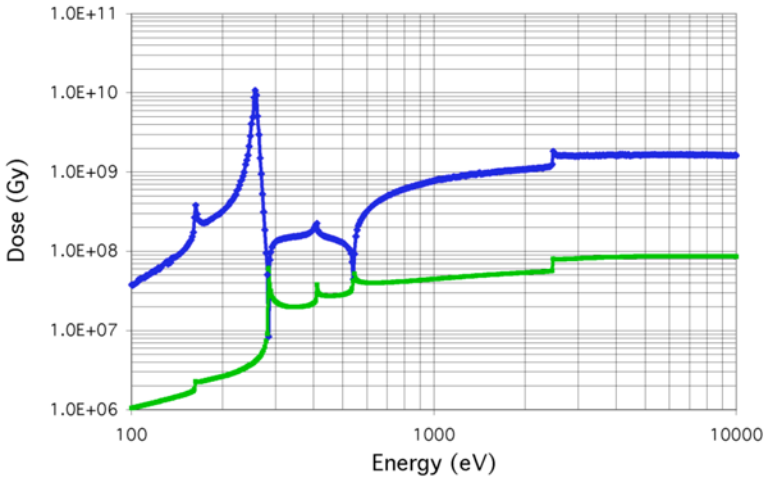

Fig. 2(b)

Fig. 2.

(a) The x-ray fluence required to visualize a 10 nm cubic voxel of protein of empirical formula $H_{50}C_{30}N_9O_{10}S_1$ and density 1.35 gm/cm^3 against a background of water (blue, upper) and vacuum (green, lower) with a statistical accuracy defined by the Rose criterion.

(b) the dose required to visualize a 10 nm cubic voxel of protein of empirical formula $H_{50}C_{30}N_9O_{10}S_1$ and density 1.35 gm/cm^3 against a background of water (blue, upper) and vacuum (green, lower) with a statistical accuracy defined by the Rose criterion.

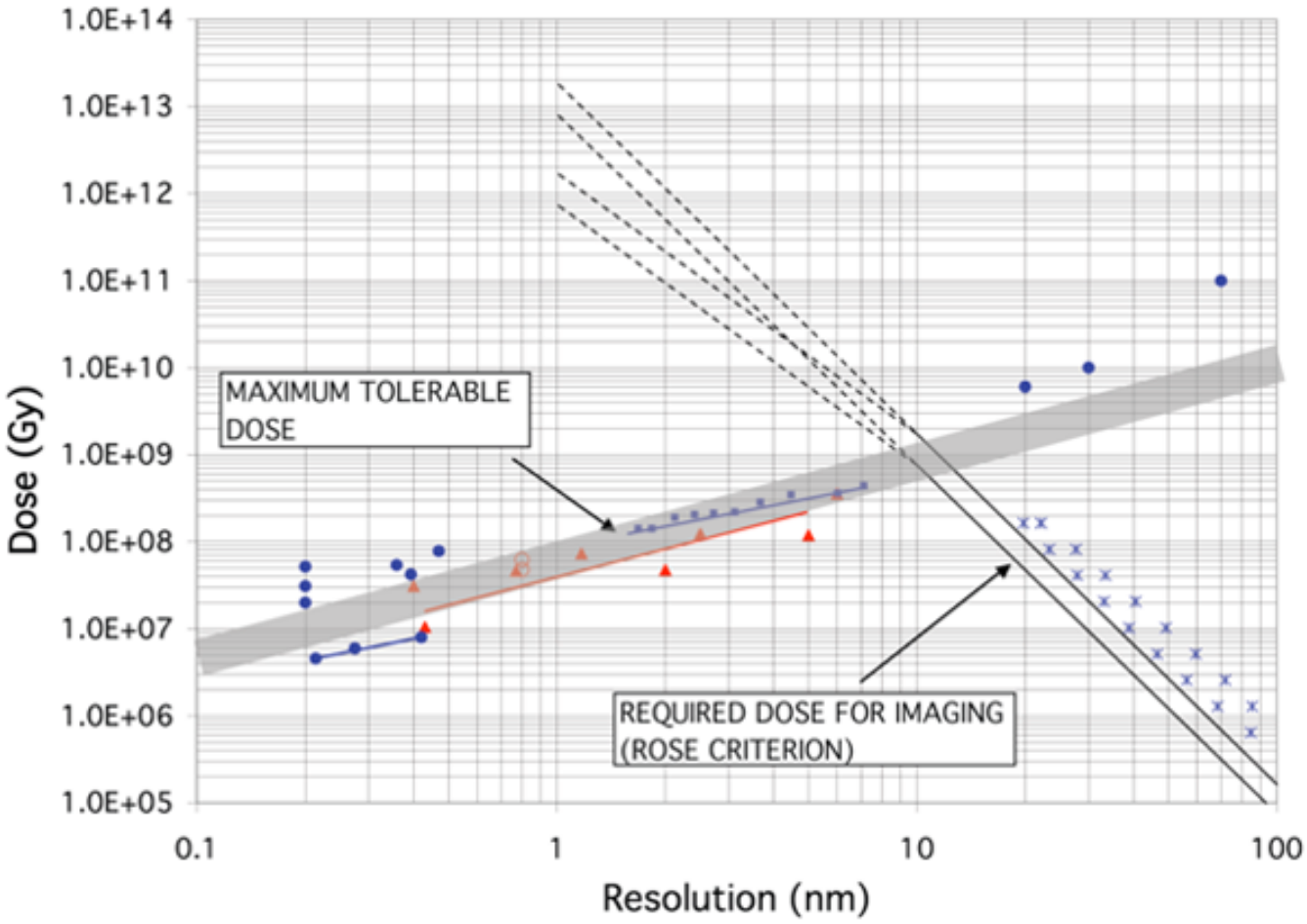

Fig. 3.

Graph summarizing information on the *required dose for imaging* and the *maximum tolerable dose*. The required dose for imaging is calculated for protein of empirical formula $H_{50}C_{30}N_9O_{10}S_1$ and density 1.35 gm/cm^3 against a background of water for x-ray energies of 1 keV (lower continuous line) and 10 keV (upper continuous line). The dashed continuations of these lines refer to the transition region from coherent (d^{-4} scaling) to incoherent (d^{-3} scaling) behavior, both of which are shown down to 1 nm resolution. Some of our measurements of the required dose for imaging are plotted as crosses (see text and Fig. 4). The maximum tolerable dose is obtained from a variety of experiments by ourselves (see text) and from the literature as described in Table 1. The types of data from the literature are identified by the symbols as follows: filled circles: x-ray crystallography, filled triangles: electron crystallography, open circles: single-particle reconstruction, open triangles: electron tomography, diamonds: soft x-ray microscopy (including XDM), filled squares: ribosome experiment (see text and Fig. 5).

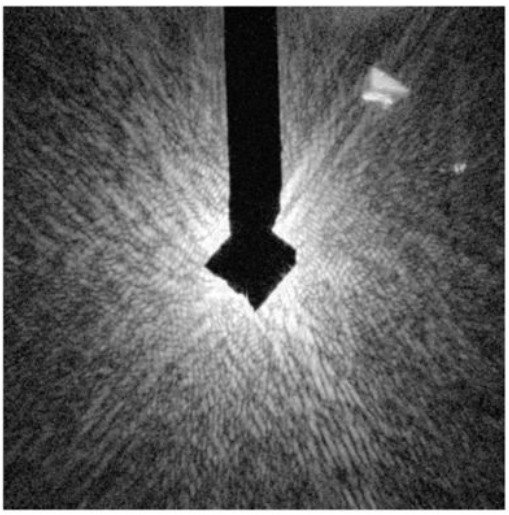

Fig. 4(a)

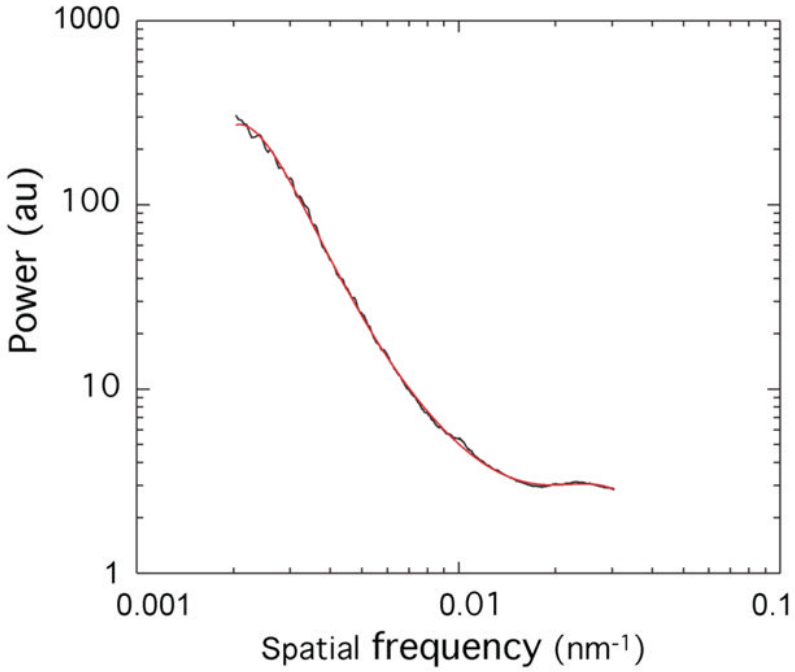

Fig. 4(b)

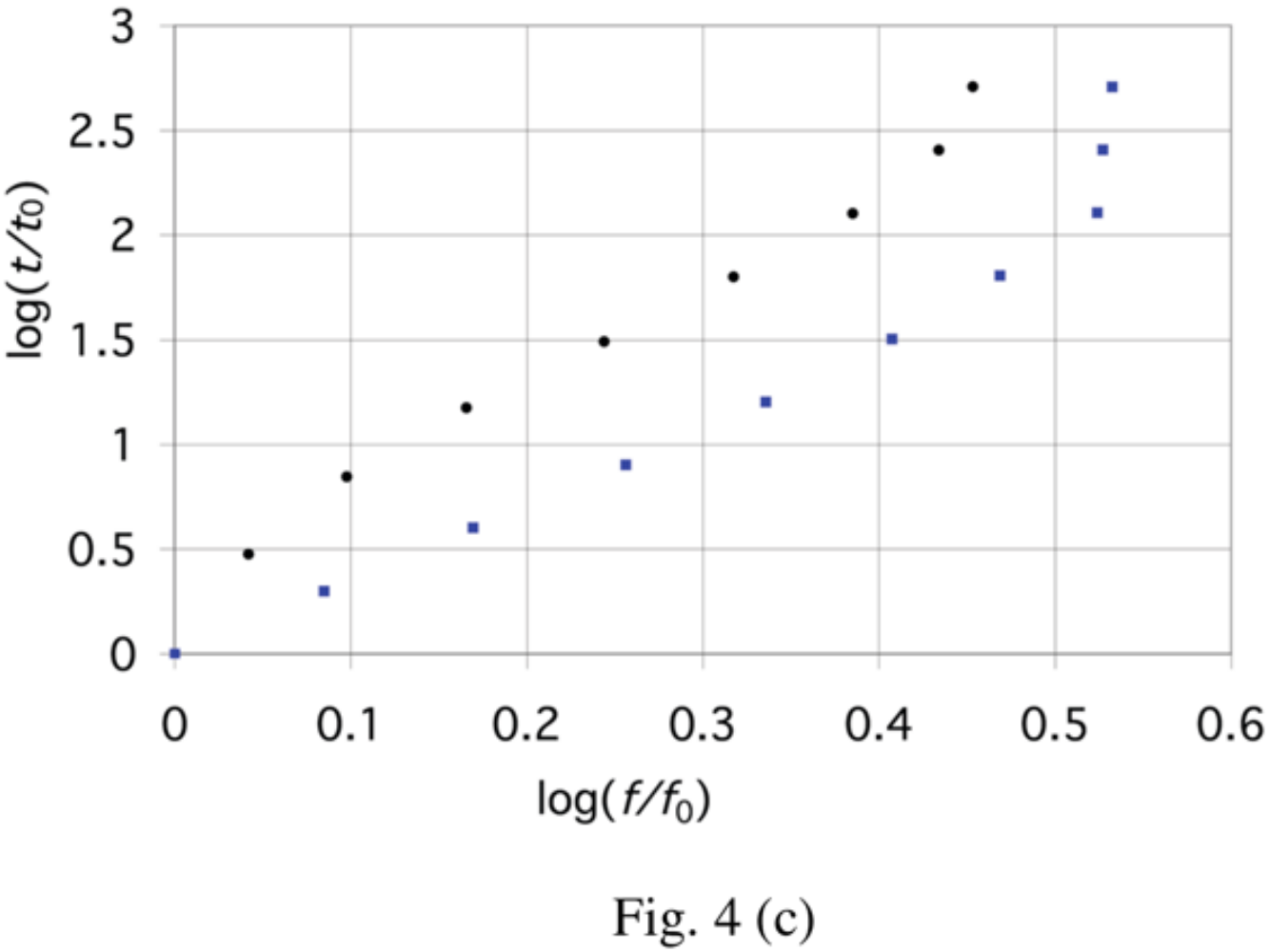

Fig. 4 (c)

Fig. 4.

Representations of steps in the experimental determination of the required dose for imaging using freeze-dried yeast cells. (a) a typical diffraction pattern, (b) a radially averaged power spectrum of a pattern (with a polynomial fit), from which the cut-off frequency can be obtained and (c) two plots of normalized cut-off frequency versus normalized dose, the meaning of which is discussed in the text.

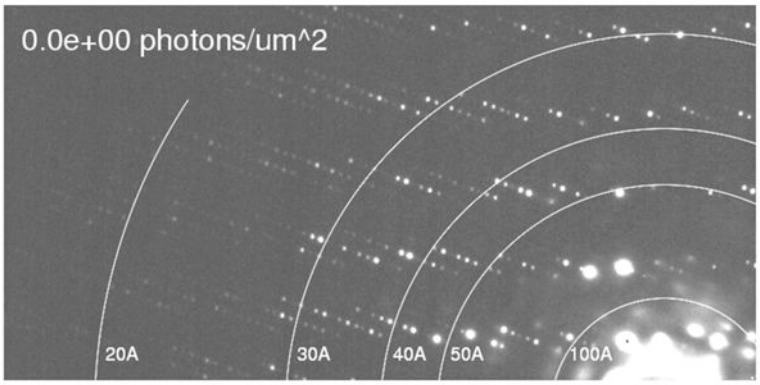

Fig. 5(a)

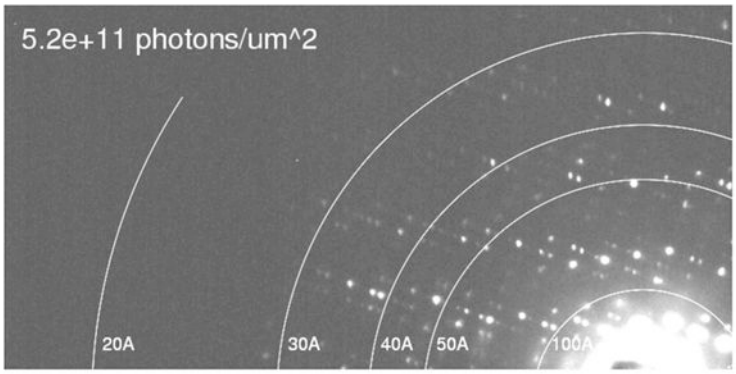

Fig 5(b)

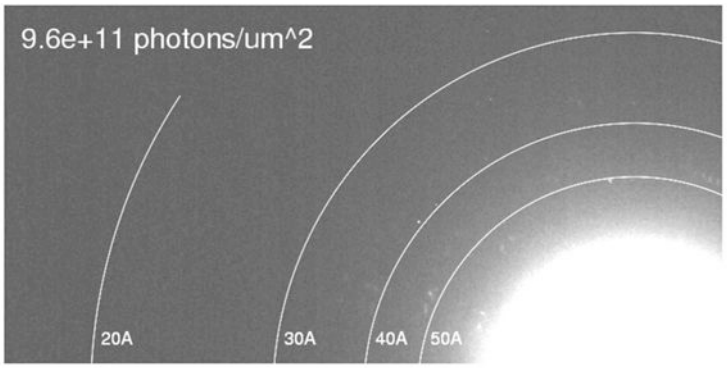

Fig. 5(c)

Fig. 5.

Three of twenty six spot patterns recorded in the spot-fading experiment described in the text. They were recorded from a ribosome crystal using beam line 8.3.1 at the Advanced Light Source at The Lawrence Berkeley National Laboratory. The accumulated dose prior to the recording is shown in the top left of the picture. Many of the spots seen at the beginning of the sequence (a) have faded by the middle (b) and essentially all are gone by the end (c). The full sequence can be seen as a movie at http://bl831.als.lbl.gov/~jamesh/ribo_blast/diffraction.gif.

TABLE 1

data types and sources used to estimate the maximum tolerable dose

Res'n (nm)	Dose (Gy)	Experiment	Particle energy (keV)	Reference	Sample: (crystal except where stated)
Electrons					
0.43	1.06E+07	spot fading	100	[17]	catalase
2.5	1.25E+08	spot fading	100	[17]	catalase
5.0	1.20E+08	tomography	300	[33,42]	cell in amorphous ice
0.77	4.67E+07	spot fading	100	[19]	purple membrane
1.17	7.35E+07	spot fading	100	[19]	purple membrane
0.4	3.12E+07	spot fading	100	[19]	purple membrane
0.8	4.80E+07	single particle reconst'n	100	[16]	protein single molecules
0.8	6.20E+07	single particle reconst'n	100	[16]	protein single molecules
X-rays					
30	1.00E+10	microscopy Berlin	0.52	[53]	cell in amorphous ice
60	5.00E+11	microscopy Brookhaven	0.52	[31]	cell in amorphous ice
0.2	2.00E+07	generic limit	8-12	[21]	organic material
0.2	3.10E+07	spot fading	13.1	[5]	myrosinase
0.36	5.40E+07	spot fading	12.4	[57]	various
0.47	7.80E+07	spot fading	12.4	[57]	various
0.39	4.20E+07	spot fading	12.4	[57]	various
25.0	3.00E+09	XDM Berkeley	0.52	this work	yeast cell freeze dried
0.42	8.00E+06	spot fading	11	[14]	bacteriorhodopsin
0.28	5.95E+06	spot fading	11	[14]	bacteriorhodopsin
0.21	4.55E+06	spot fading	11	[14]	bacteriorhodopsin
7.1	4.44E+08	spot fading	10	this work	ribosome
6.0	3.64E+08	spot fading	10	this work	ribosome
4.5	3.49E+08	spot fading	10	this work	ribosome
3.7	2.85E+08	spot fading	10	this work	ribosome
3.1	2.22E+08	spot fading	10	this work	ribosome
2.7	2.14E+08	spot fading	10	this work	Ribosome

Res'n (nm)	Dose (Gy)	Experiment	Particle energy (keV)	Reference	Sample: (crystal except where stated)
2.4	2.06E+08	spot fading	10	this work	ribosome
2.1	1.90E+08	spot fading	10	this work	ribosome
1.8	1.43E+08	spot fading	10	this work	ribosome
1.7	1.43E+08	spot fading	10	this work	ribosome